# 3D-SLIP Steering for High-Speed Humanoid Turns

Patrick M. Wensing and David E. Orin

***Abstract*— This paper presents new methods to control humanoid turns while running, through the use of a 3D-SLIP template model with steering control. The work builds on a previous controller for straight-ahead running and describes the new methods that enable online humanoid steering for different speeds and turn rates. As opposed to previous research which has studied 3D-SLIP steering with a monopod model, motion optimization for the SLIP here enforces leg separation. This leg separation gives rise to body sway in forward running and allows the template to capture the unique roles that the inside and outside legs each play during a high-speed turn. The trajectory optimization approach for this template is given, and the resultant CoM trajectories are characterized. Modifications to a previous controller for straight-ahead running are shown to enable running turns in a simulated humanoid model. The methods allow the humanoid to change its turn rate and direction from step to step and enable execution of a high-speed turn with a radius that is one fourth that of a standard 400m track. A video attachment to this paper shows the humanoid turning while running at up to 4.0 m/s, and highlights its ability to maintain balance in spite of push disturbances.**

## I. Introduction

Despite significant research into humanoid robots over the past 15 years, these systems have yet to demonstrate significant maneuverability or agility. While a portion of this problem can be attributed to actuation and sensing challenges that face current humanoids, the development of control methods for fast, maneuverable locomotion remains an open problem. During high-speed dynamic locomotion, the humanoid must reason about the long term consequences of discrete actions that it takes, namely in the selection of its footholds. Although it is difficult to reason about the high-dimensional nonlinear dynamics of the humanoid over any significant time frame, it is common to employ simple template models such as the Linear Inverted Pendulum [1] in walking or the Spring-Loaded Inverted Pendulum (SLIP) in hopping or running [2], [3] in order to make long-term planning practical.

The use of these template models allows step-level control to focus on the most important characteristics of a motion, such as the Center of Mass (CoM), while continuous controllers can be designed to embed the low-dimensional dynamics encoded in the template. In this paper, the problem of steering a 3D-SLIP model [4] is studied in order to enable real-time control of humanoid turning in simulation. In order for the SLIP footholds to be kinematically accessible when retargeted to the humanoid, leg separation is enforced, which gives rise to unique roles for each leg during the turn.

P. M. Wensing is a PhD student in the Department of Electrical and Computer Engineering, The Ohio State University: wensing.2@osu.edu

D. E. Orin is a Professor Emeritus in the Department of Electrical and Computer Engineering, The Ohio State University: orin.1@osu.edu

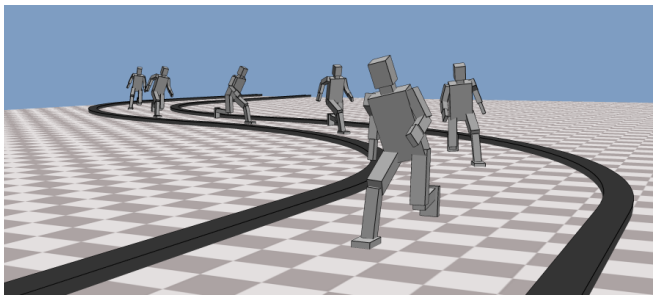

Fig. 1. This paper describes methods for online control of humanoid turning. The use of a 3D-SLIP template model with steering control allows a knowledge base to be developed for humanoid running control at different speeds and turning rates. CoM trajectories generated from this knowledge base are tracked online with a whole-body task-space controller which uses torque control at the humanoid joints.

3D-SLIP steering control has been addressed for single leg models by a variety of other authors. Recent work by Wu and Geyer [5] has studied 3D-SLIP steering and discovered time-based deadbeat control laws that provide terrain robustness to the template. These laws extend their previous results of 2D-SLIP hopping with time-based deadbeat control [6]. While the methods in this paper are not presently robust to terrain variation, a synergy with the ideas in [5] could be an interesting avenue to provide future terrain robustness. Carver [7] studied a variety of 3D-SLIP steering problems for a single leg model, but also did not focus on trajectories that could be retargeted to a humanoid.

Overall, very little work has been done on executing dynamic turns for humanoid robots. An exception is the recent work by Miura et al. [8] which has focused on controlling an in-place turn wherein the feet slip rotationally with respect to the ground. The running turn executed here faces challenges that are largely distinct from an in-place turn. Due to its non-zero turn radius, a significant centripetal force is required to execute the turn. In simulation, Hodgins et al. [9] developed running turns for human characters through a series of heuristically designed controllers. Palmer and Orin [10] studied fuzzy control methods for a turn in a quadruped trot. Krasny and Orin [11] developed a turn during a quadruped gallop using computationally intensive offline genetic algorithms. Mordatch et al. [12] used online optimization with a novel template to generate turns during a humanoid walk. The use of the 3D-SLIP to execute a humanoid running turn here is a new feature in comparison to previous work, allowing higher speed locomotion in comparison to [12] and requiring less intensive heuristic design in comparison to [9].

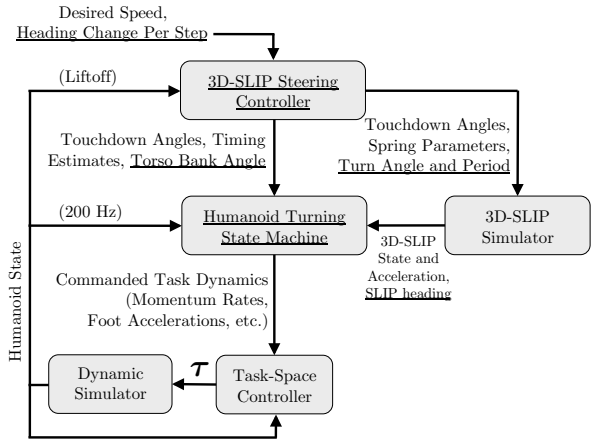


Fig. 2. Block diagram for the humanoid control system with 3D-SLIP CoM steering. The structure is similar to [3], with the main changes for turning underlined. A step controller based on the 3D-SLIP model is used to find touchdown angles and SLIP-spring parameters for the next step. These parameters then drive a 3D-SLIP simulation to provide CoM trajectories online. The turning state machine here uses the principal heading direction of the 3D-SLIP to shape commands to the task-space controller.

The remainder of this paper is organized as follows. Section II introduces the 3D-SLIP model and a new notion of its principal heading direction. Section III then presents an optimization-based approach to generate 3D-SLIP trajectories for a turn. Methods to track the resultant trajectories are presented in Section IV with many details left to previous work [3]. Fig. 2 provides a summary of the main changes to this previous control architecture which enable humanoid turns here. The results in Section V describe how the new methods allow the inside and outside legs to play specialized roles during the turn. Namely, the outside leg produces the majority of the centripetal force to execute the turn, while the inside leg largely only supports the weight of the humanoid. These roles are consistent with the kinematic ability of each leg to generate centripetal force, and are a consequence of the 3D-SLIP optimization proposed. This result is the main contribution of the paper, as previous 3D-SLIP steering approaches have not addressed the ability to realize their trajectories in a two-leg morphology.

## II. 3D-SLIP Model

Planar spring-mass models of locomotion have been shown to describe the Center of Mass (CoM) dynamics well across a wide range of species [13]. As one of the simplest of these models, the common Spring-Loaded Inverted Pendulum (SLIP) model has been widely studied and applied in biomechanics and robotics over the past 25 years. In order to capture out-of-plane effects, this planar model has been extended to three dimensions [4], which has proven to be valuable in the development of control methods for straight-ahead humanoid running [3]. In this work, the 3D-SLIP model is adopted to generate target CoM dynamics for the humanoid during a turn through 3D-SLIP steering.

### A. Continuous Dynamics

The 3D-SLIP model used here is in many parts the same as that used in straight-ahead running [3]. As a main

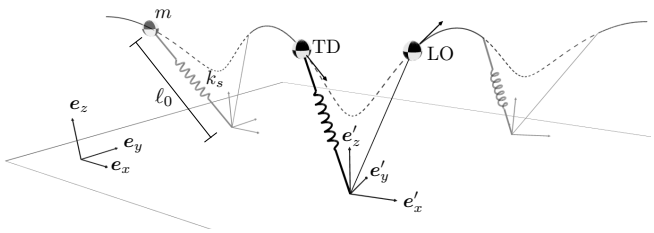


Fig. 3. In order to model the forward heading direction of the 3D-SLIP model during motions with lateral sway, an auxiliary coordinate system $\boldsymbol{e}'_x$, $\boldsymbol{e}'_y$, $\boldsymbol{e}'_z$ is associated with the template. This coordinate system rotates as the 3D-SLIP mass changes its principal heading relative to the fixed inertial coordinates $\boldsymbol{e}_x$, $\boldsymbol{e}_y$, $\boldsymbol{e}_z$. While this primed coordinate system doesn't affect the dynamics of the 3D-SLIP, it is used by the whole-body humanoid control to distinguish between the pitch (about $\boldsymbol{e}'_y$) and roll (about $\boldsymbol{e}'_x$) components of the humanoid's orientation.

difference, a supplementary coordinate system is included in the template to capture the principal heading direction of its mass during a a turn. This supplementary coordinate system $\boldsymbol{e}'_x$, $\boldsymbol{e}'_y$, $\boldsymbol{e}'_z$ is shown in Fig. 3 and rotates, about the inertial $\boldsymbol{e}_z$ axis, as the 3D-SLIP mass changes its principal direction of travel. It is important to note that due to effects of lateral sway, the $\boldsymbol{e}'_x$ forward heading coordinate is not generally aligned with the velocity of the SLIP mass. The orientation of this prime coordinate system is given with respect to the inertial coordinate system (ICS) $\boldsymbol{e}_x$, $\boldsymbol{e}_y$, $\boldsymbol{e}_z$ by the rotation matrix:

$$\boldsymbol{R}_s(\gamma) = \begin{bmatrix} \cos(\gamma) & -\sin(\gamma) & 0 \\ \sin(\gamma) & \cos(\gamma) & 0 \\ 0 & 0 & 1 \end{bmatrix}, \tag{1}$$

where $\gamma$ represents the principal heading angle.

The point-mass model shown in Fig. 3 experiences alternating periods of ballistic flight followed by stance. The position of the mass $m$ is given in inertial coordinates as $\boldsymbol{p}_s \in \mathbb{R}^3$ with velocity $\dot{\boldsymbol{p}}_s \in \mathbb{R}^3$. Flight dynamics follow $m\,\ddot{\boldsymbol{p}}_s = m\,\boldsymbol{g}$, where $\boldsymbol{g} \in \mathbb{R}^3$ is the gravity vector. In stance, the mass $m$ is driven by a linear spring with rest length $\ell_0$ and spring constant $k_s$.

Similar to our previous approach, the foot position $\boldsymbol{p}_f \in \mathbb{R}^3$ is adjusted in flight for the upcoming stance with touchdown angles $\theta$ and $\boldsymbol{\phi}$ as

$$\boldsymbol{p}_f = \boldsymbol{p}_s + \boldsymbol{R}_s \cdot \left( \boldsymbol{p}_{hip} + \ell_h \begin{bmatrix} \sin(\theta)\cos(\phi) \\ -\sin(\theta)\sin(\phi) \\ -\cos(\theta) \end{bmatrix} \right) . \tag{2}$$

Here $\ell_h$ represents the length of the humanoid virtual leg (hip to foot center) at touchdown, and $\boldsymbol{p}_{hip}$ is the position of the hip with respect to the CoM. The quantity $\theta$ controls the angle between the humanoid virtual leg and the $\boldsymbol{e}'_z$ axis, while $\phi$ rotates the leg laterally outward about the $\boldsymbol{e}'_z$ axis. In the special case when $\phi = 0$, the foot is placed directly in front of the hip along the $\boldsymbol{e}'_x$ direction. By placing suitable bounds on $\theta$ and $\phi$, the hip separation $\boldsymbol{p}_{hip}$ enforces a limited kinematic workspace for the foot. Flight ends at touchdown (TD) when the foot intersects the ground plane.

In stance, the dynamics follow

$$m\,\ddot{\boldsymbol{p}}_s = k_s(\ell_0 - ||\boldsymbol{\ell}||)\,\hat{\boldsymbol{\ell}} + m\,\boldsymbol{g} \tag{3}$$

where $\ell_0$ is the rest length of the spring (computed as its length at touchdown), $\boldsymbol{\ell} \in \mathbb{R}^3$ is given by $\boldsymbol{\ell} = \boldsymbol{p}_s - \boldsymbol{p}_f$, and $\hat{\boldsymbol{\ell}}$ is the unit vector along $\boldsymbol{\ell}$. Stance ends at liftoff (LO), when the leg has returned to its rest length.

### B. Discrete Dynamics

While the continuous dynamics of the 3D-SLIP model will be needed to generate continuous CoM trajectories online, the discrete step-to-step dynamics of this model will be useful to generate step controllers. Here, discrete control will be limited to a slice of the SLIP state $\mathbf{x}$ at Top of Flight (ToF) which includes the CoM velocity and height:

$$\mathbf{x} = \left[\boldsymbol{e}_x^T \dot{\boldsymbol{p}}_s,\ \boldsymbol{e}_y^T \dot{\boldsymbol{p}}_s,\ \boldsymbol{e}_z^T \boldsymbol{p}_s\right]^T \ . \tag{4}$$

Starting from a ToF state $\mathbf{x}_n$ with assumed heading $\boldsymbol{R}_s = \boldsymbol{\Sigma}_n$, the touchdown angles $\theta$, $\phi$ and leg spring constant $k_s$ can be selected to steer the model to a desired state $\mathbf{x}_{n+1}$ at the following ToF. Given a selection of control variables $\mathbf{u}_n = [\theta, \phi, k_s]^T$, forward simulation of the continuous dynamics can be used to determine the next ToF state, which is described here by the return map $\mathbf{f}$ as:

$$\mathbf{x}_{n+1} = \mathbf{f}(\mathbf{x}_n, \boldsymbol{\Sigma}_n, \mathbf{u}_n). \tag{5}$$

Due to the structure of $\boldsymbol{R}_s$, this return map obeys:

$$\mathbf{f}(\mathbf{x}_n, \boldsymbol{\Sigma}_n, \mathbf{u}_n) = \boldsymbol{\Sigma}_n \, \mathbf{f}(\boldsymbol{\Sigma}_n^T \mathbf{x}_n, \mathbf{I}, \mathbf{u_n}), \tag{6}$$

where $\mathbf{I}$ is the identity matrix. This equation amounts to performing simulation in ToF local coordinates, and then rotating the result back into the ICS.

## III. 3D-SLIP Steering Optimization

This section introduces a principled optimization-based approach to find 3D-SLIP controls $\mathbf{u}$ for running at a given speed and turning rate. As opposed to forward running, separate controls are required for inside and outside legs during a turn. The unique role played by the inside and outside legs is a new property of the 3D-SLIP optimization proposed here. Optimized trajectories for a given forward speed are designed to maintain continuity when transitioning to and from any turn rate. This design enables online humanoid steering with step-to-step modifications in the turn rate. Previous results for straight-ahead running are first summarized, which allows for consideration of the special case of transitions from straight-ahead running into a turn.

### A. 3D-SLIP Trajectories for Straight-Ahead Running

Given a desired forward speed $v_x$, 3D-SLIP optimization approaches for straight-ahead running [3] provide a ToF state $\mathbf{x}^* = [v_x, v_y^*, h^*]^T$ and control variables $\mathbf{u}^* = [\theta^*, \phi^* = 0, k_s^*]^T$ for periodic 3D-SLIP running. These parameters allow the humanoid to run with its feet placed in front of its hips when trajectories are retargeted. It is key to note that this footstep separation gives rise to lateral CoM sway with velocity $v_y^*$ at ToF. Letting $\mathbf{A} \in \mathbb{R}^{3\times 3}$ be diagonal with entries $[1, -1, 1]$. The ToF state-control pair is optimized to satisfy:

$$\mathbf{A}\,\mathbf{x}^* = \mathbf{f}(\mathbf{x}^*, \mathbf{I}, \mathbf{u}^*) \tag{7}$$

which enforces 1-step periodicity on the ToF height $h$ and forward velocity $v_x$, but 2-step periodicity on the ToF lateral velocity $v_y$. As a matter of convention, $\mathbf{x}^*$ is selected to represent the ToF state prior to a left foot stance, while the ToF state before a right foot stance is given by $\mathbf{A}\mathbf{x}^*$.

### B. Transitions from Straight-Ahead Running into a Turn

As a special case, consider the situation of starting from a periodic run with forward speed $v_x$. Given the state-control pair for straight-ahead running $(\mathbf{x}^*, \mathbf{u}^*)$, new control inputs must be employed to start from $\mathbf{x}_0 = \mathbf{x}^*$ and execute a turn. Here, as one possible approach, the rate of turning is characterized by a change in heading angle $\Delta\gamma$ per step. The method proposed here enforces this turn angle by selecting left foot and right foot parameters $\mathbf{u}_L$ and $\mathbf{u}_R$ such that

$$\boldsymbol{R}_s(\Delta\gamma)\,\mathbf{A}\,\mathbf{x}_0 = \mathbf{f}(\mathbf{x}_0, \mathbf{I}, \mathbf{u}_L), \tag{8}$$

$$\boldsymbol{R}_s(2\Delta\gamma)\,\mathbf{x}_0 = \mathbf{f}(\mathbf{A}\,\mathbf{x}_0, \boldsymbol{R}_s(\Delta\gamma), \mathbf{u}_R)\ . \tag{9}$$

This design choice will be shown to produce Ground Reaction Force (GRF) patterns that are consistent with the kinematic ability of each leg to produce centripetal force. While the turn angle $\Delta\gamma$ is only enforced on velocity, it can be shown that the resultant CoM positions have a sweep angle of $2\Delta\gamma$ from ToF to ToF following a left and right foot cycle. A formal proof will be provided in a future publication, which follows from the ability to sequentially compose rotated trajectories which obey (8) and (9).

Intuitively, if the condition (8) is satisfied, the next ToF velocity w.r.t. local coordinates will be numerically equal to the ToF velocity w.r.t. the ICS during forward running. This property allows the resultant CoM trajectory to be smoothly composed with that for any new turn rate in the following step. However, this condition also enforces alternating lateral sway velocities (in local coordinates) from step to step during the turn. While this may seem like a drawback, because it allows sway to the outside of the turn on every other step, the results in Section V show that this design decision allows each leg to make proper use of its kinematic availability to generate centripetal force during the turn.

To find such a $\mathbf{u}_L$ which satisfies (8), the following optimization problem is formulated:

$$\min_{\theta,\phi} \ \|\boldsymbol{R}_s(\Delta\gamma)\,\mathbf{A}\,\mathbf{x}_0 - \mathbf{f}(\mathbf{x}_0, \mathbf{I}, \mathbf{u})\|^2 \tag{10}$$

$$\text{s.t. } \mathbf{u} = [\theta, \phi, k_s^*]^T \tag{11}$$

$$\underline{\theta} \le \theta \le \overline{\theta} \tag{12}$$

$$\underline{\phi} \le \phi \le \overline{\phi}\,, \tag{13}$$

where the $\underline{\cdot}$ and $\overline{\cdot}$ symbols represent bounds summarized in Table I. The selection of a fixed leg stiffness equal to that in forward running ($k_s^*$) has been found to simplify optimization and result in comparable gait timings to forward running. This optimization problem can be solved quickly (usually under a second with an appropriate initial guess) in MATLAB using the nonlinear least squares function `lsqnonlin`. Turn amounts $\Delta\gamma$ are determined to be valid in the case that the objective function is zero at the optimum.

| Variable | Lower Bound | Upper Bound |
|---|---|---|
| $\theta$ | 0 | $\pi/4$ |
| $\phi$ | $-\pi/2$ | $\pi/2$ |

TABLE I

KINEMATIC BOUNDS PLACED ON THE HUMANOID VIRTUAL LEG ANGLES FOR 3D-SLIP OPTIMIZATION

Due to property (6), the same optimization can be repeated with $\mathbf{x}_0 = \mathbf{A}\mathbf{x}^*$ to obtain $\mathbf{u}_R$ for the right leg. This process is repeated offline for a range of forward speeds and turn amounts. These pre-optimized turns can then be composed in real-time through 3D-SLIP simulation using the stored control parameters.

As in previous work [3], 3D-SLIP feedback controllers can be constructed to stabilize the CoM dynamics of the humanoid when they deviate from the 3D-SLIP trajectories. In this manner, the state of the 3D-SLIP can be periodically reset to match the CoM state of the humanoid, while SLIP-based trajectories are generated online to return to the desired CoM motion. Feedback methods similar to [3] were replicated here to provide SLIP-based recovery trajectories through online modification of the nominal pre-optimized controls $\mathbf{u}_L$ and $\mathbf{u}_R$. Although space does not permit a full exposition into the method and its modification, the main idea is to compute separate linear feedback matrices $\mathbf{K}$ automatically for each speed, turning rate, and leg. In practice, however, we have found the SLIP feedback matrices $\mathbf{K}$ for straight-ahead running to be sufficient across a wide range of turn rates. Future publication will detail this method further.

## IV. HUMANOID MODEL AND CONTROL

The humanoid model used in this work, shown in Fig. 1, is a 26 degree of freedom (DoF) model, with 20 actuated DoFs. It is modeled after a 6 foot, 160 pound male. The mass distribution to each segment is modeled after a 50-th percentile male, with further details provided in [14]. This reference also contains a description of the 3D dynamic simulation environment used here.

Control of this high degree-of-freedom model is accomplished through the combination of a Turning State Machine and a Task-Space controller to track the 3D-SLIP CoM reference trajectories and stabilize the remainder of the system (Fig. 2). The task-space controller from [14] is used here without modification and enables real-time control of the humanoid for different turn rates and speeds when used with the Turning State Machine.

The main characteristics of the Turning State Machine are similar to straight-ahead running. Namely, CoM and centroidal angular momentum control are applied during stance to control balance, while foot position and orientation control is applied throughout to track hand-designed foot trajectories. The main design change here is that a number of the control targets are judiciously selected to occur w.r.t. the $\boldsymbol{e}'_x$, $\boldsymbol{e}'_y$, $\boldsymbol{e}'_z$ coordinate system. These control targets are then realized through a prioritized-task space controller that selects joint torques and ground reaction forces.

### A. Stance Control

Stance control is comprised of CoM, centroidal angular momentum, foot, and pose control. The commanded foot dynamics are set as the highest priority. While a foot in stance is given a zero acceleration command, a PD control law with feedforward is used to generate the commanded flight foot dynamics. Flight foot trajectories are generated online using cubic splines for the position of the foot relative to the CoM. By applying this control w.r.t. the rotating coordinate system associated with the 3D-SLIP, leg trajectories for forward running are able to be applied to the case of the turn.

CoM and centroidal angular momentum control is again applied to maintain balance. CoM control is carried out w.r.t. the ICS, while centrioidal angular momentum is controlled about the rotating SLIP coordinates. Centroidal angular momentum control is applied with a setpoint,

$$\boldsymbol{k}_{G,d} = [0, 0, I_{zz}\omega]^T, \tag{14}$$

where $I_{zz}$ is the system's net moment of inertia about the $\boldsymbol{e}'_z$ axis, and $\omega$ is computed from $\Delta\gamma$ and the gait period. During running, leg cycling in the sagittal plane causes pitch angular momentum to oscillate with a non-zero average value. Since this quantity is not well regulated to any particular value during human running, angular momentum control is only applied w.r.t. the $\boldsymbol{e}'_x$ and $\boldsymbol{e}'_z$ coordinate axes.

Finally, pose control is applied with a low task weight to promote a natural configuration of the system. As the main difference during the turn, a rolled orientation set point of the torso relative to $\boldsymbol{e}'_x$ is selected to provide a banked turn. The banked roll angle is chosen based on the roll angle of the humanoid virtual leg found from 3D-SLIP optimization. Proper selection of this bank angle keeps the hip angles close to kinematically centered, which provides maximum kinematic availability to respond to any disturbances.

### B. Flight Control

Control during flight is largely the same as stance with two main differences. First, CoM and centroidal angular momentum control are disabled. Secondly, foot trajectory servos relative to the CoM in local coordinates are applied for both legs in flight. The discrete nature of the 3D-SLIP ToF to ToF dynamics requires one additional modification. As a practical implementation issue, the SLIP simulator is augmented with a continuous heading trajectory generator based on a cubic spline. This cubic spline is initialized to match the angle of the discrete rotations of the $\boldsymbol{e}'_x$, $\boldsymbol{e}'_y$, $\boldsymbol{e}'_z$ system that change at ToF. The use of this spline prevents discrete changes in the control objectives at ToF.

## V. RESULTS

### A. Continuous Turning

Continuous turning with a forward speed of 3.5 m/s and a turn rate of $\omega = 0.4$ rad/s is highlighted here and in the video attachment. The video is also available online at:

`http://www.go.osu.edu/Wensing_Orin_IROS2014`

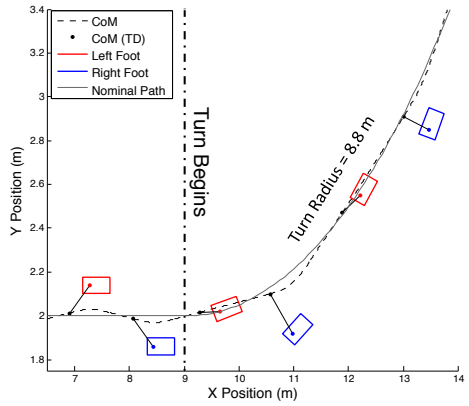


Fig. 4. Foot positioning used by the humanoid for a running turn at 3.5 m/s with a turning rate of $\omega$=0.4 rad/s. The nominal path for the turn is a circle with radius that is approximately 1/4 that of the inside-most lane of a 400m track. Both feet are placed towards the outside of the turn to generate the inward radial force required to execute the turn. However, radial force production is different for each leg, as lateral sway about the nominal path enables all footholds to remain kinematically reachable.

The foot positions applied by the humanoid for this turn are shown in Fig. 4. During a straight-ahead portion before the turn, the feet are placed directly in front of the hips. When the turn begins, touchdown angles pre-optimized as $\mathbf{u}_L$ and $\mathbf{u}_R$ for this turn rate are used to execute the turn. Both feet are placed towards the outside of the curve in order to generate additional centripetal force in comparison to forward running. It can be seen that curvature of the CoM trajectory during a right foot stance is much higher than during a left foot stance. In this sense, the right leg is doing more work to accomplish the turn than the left leg.

To understand this effect further, the lateral ground reaction forces (GRFs) were compared between straight-ahead running and during the turn. In Fig. 5 for straight-ahead running, the lateral force alternates from positive in one step to negative in the next. This pattern gives rise to lateral CoM sway and enables foot placement in front of the hips. When transitioning to the turn, with forces in Fig. 6, the forces in the forward direction are largely unchanged. However, in the lateral direction, both feet provide additional force towards the center of the turn in comparison to forward running. Although the left foot produces much less centripetal force to execute the turn, it is kinematically unavailable to produce the same forces as the right foot. That is, to execute a left turn, centripetal forces are generated by placing the foot to the right of the CoM. Since it is kinematically difficult for the left foot to be placed to the right of the CoM, any valid foot placement strategy for a left turn will result in the left foot having less authority to generate centripetal force. The approach here results in different roles for the inside and outside legs that are consistent with this limitation. In contrast, application of trajectories from monopod steering would employ the same outward foot positioning relative to the CoM at each step. This would result in footholds that are not reachable by the humanoid's inside leg.

The plots in Fig. 7 show how this foot placement varies as speed and turn rate are increased. Simple physics dictates

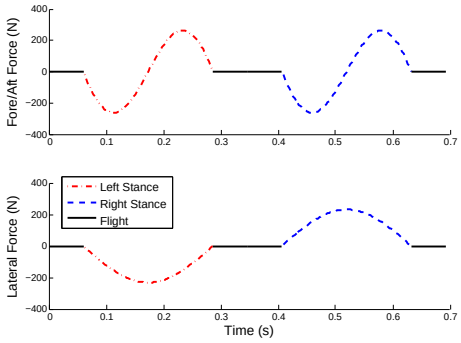


Fig. 5. Force profiles for 3.5 m/s running with the 3D-SLIP template. The two-step periodic nature of the lateral force provides a two-step period to the lateral CoM dynamics. The CoM enters the left step with a lateral velocity toward the left foot (in the $\boldsymbol{e}_y$ direction). As a result of the left foot force in stance, this velocity is reversed in sign by the following LO.

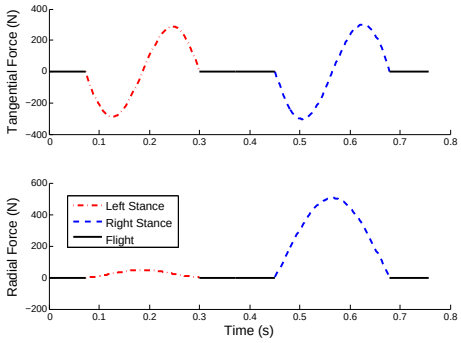


Fig. 6. Force profiles for 3.5 m/s running and a 0.4 rad/s turn rate to the left. While the tangential ($\boldsymbol{e}'_x$) force is largely the same as the fore/aft force for forward running, the radial ($\boldsymbol{e}'_y$) force is more positive for both feet.

that the centripetal force required for the turn will scale proportional to the product $v_x\omega$. These trends are observed in the foot placements as speed or turn rate is increased. With higher speed or turn rate, the touchdown angles are optimized to place the feet further toward the outside of the turn. Note that in all of the cases shown in this figure, the left foot produces forces towards the outside of the curve. It is only at higher speeds or turn rates as in Fig. 4 that the direction of curvature for the CoM trajectory during left foot stance matches that of the nominal circular path followed.

### *B. Online Steering with Different Turn Rates*

The design approach taken in Section III allows the humanoid turn rate to be modified online from step to step without any additional required 3D-SLIP optimization. To demonstrate the ability to compose trajectories of different turn rates, the extreme case of switching turn direction in a single step is illustrated in the video attachment to this paper.

In this demonstration, the humanoid runs at $4.0$ m/s with a turn rate of $\omega = 0.3$ rad/s. Following the execution of a partial turn, the commanded turn rate is changed in sign, and a new target CoM trajectory is generated online based on this new command. Actual rate commands to the 3D-SLIP are delayed by one gait cycle in order to allow the banked torso

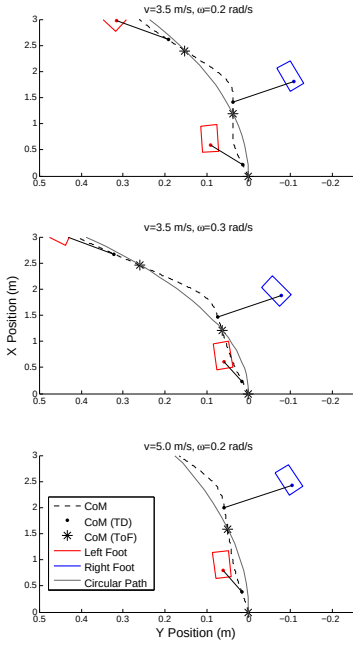


Fig. 7. Foot positioning comparison for different turn rates and running speeds. The required inward radial force to execute the turn is proportional to the product $v_x\omega$. As a result, the lateral foot placement becomes more extreme for higher turning rates and running speeds.

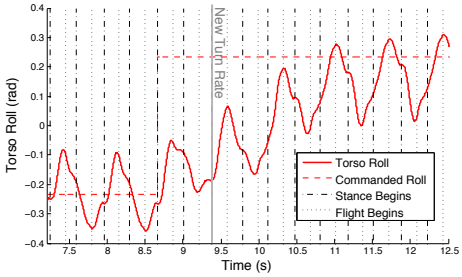


Fig. 8. Torso roll during a left turn to right turn transition. A new torso orientation is commanded one full gait cycle before the turn rate change to prepare the torso for the upcoming footstep repositioning.

roll to prepare for the upcoming change in leg angles. The tracking of the torso roll command is shown in Fig. 8 and successfully re-aligns the torso to the new leg angles within a few steps. The use of a soft PD controller on the torso prevents rapid upper body movements which would require excessive forces and potentially destabilize the system.

While it is not a main focus of this paper, the video also showcases the ability of the 3D-SLIP controller to generate recovery trajectories online in response to push disturbances. These disturbances can occur in any direction (in or out of the sagittal plane), although disturbances directed towards the center of the turn are more easily handled than those to the outside of the turn. This is an intuitive result, as proper execution of the turn depends largely on the production of centripetal force, so any disturbance towards the inside makes the turn easier to execute.

## VI. Summary

This paper has presented new methods which enable online high-speed humanoid turning. By starting from top of flight (ToF) states from straight-ahead running with leg separation, the trajectories for turning allow each leg to play a unique role during the turn. While this leads to asymmetric radial force production by the inner and outer leg, the centripetal force required for each leg is consistent with its kinematic ability to produce force in that direction. With a few judicious modifications to the control architecture for straight-ahead running, these 3D-SLIP trajectories can be followed by the humanoid. The design choices applied allows the trajectories to be smoothly combined, which gives the humanoid the ability to change turn rates online from step-to-step, and to recover from push disturbances. Future work will characterize the robustness of the approach to modeling errors such as control delay and parameter uncertainty. In addition, the use of online 3D-SLIP trajectory optimization could be studied to provide further robustness.

## VII. Acknowledgments

This work was supported by a National Science Foundation Graduate Research Fellowship to Patrick Wensing, and by Grant No. CNS-0960061 from the NSF with a subaward to The Ohio State University.

## References

[1] S. Kajita, F. Kanehiro, K. Kaneko, K. Yokoi, and H. Hirukawa, "The 3D linear inverted pendulum mode: a simple modeling for a biped walking pattern generation," in *Proc. of the IEEE/RSJ Int. Conf. on Intelligent Robots and Systems*, vol. 1, pp. 239–246, 2001.

[2] I. Poulakakis and J. Grizzle, "The spring loaded inverted pendulum as the hybrid zero dynamics of an asymmetric hopper," *IEEE Transactions on Automatic Control*, vol. 54, pp. 1779–1793, Aug. 2009.

[3] P. M. Wensing and D. E. Orin, "High-speed humanoid running through control with a 3D-SLIP model," in *Proc. of the IEEE/RSJ Int. Conf. on Intelligent Rob. and Sys.*, pp. 5134–5140, Nov. 2013.

[4] J. E. Seipel and P. Holmes, "Running in three dimensions: Analysis of a point-mass sprung-leg model," *The International Journal of Robotics Research*, vol. 24, no. 8, pp. 657–674, 2005.

[5] A. Wu and H. Geyer, "The 3-D spring–mass model reveals a time-based deadbeat control for highly robust running and steering in uncertain environments," *IEEE Transactions on Robotics*, vol. 29, no. 5, pp. 1114–1124, 2013.

[6] M. Ernst, H. Geyer, and R. Blickhan, "Spring-legged locomotion on uneven ground: A control approach to keep the running speed constant," in *12th Int Conf on Climbing and Walking Robots (CLAWAR)*, pp. 639–644, 2009.

[7] S. Carver, *Control of a Spring Mass Hopper*. PhD thesis, Cornell University, Ithaca, NY, 2003.

[8] K. Miura, F. Kanehiro, K. Kaneko, S. Kajita, and K. Yokoi, "Slip-turn for biped robots," *IEEE Transactions on Robotics*, vol. 29, pp. 875–887, Aug 2013.

[9] J. K. Hodgins, W. L. Wooten, D. C. Brogan, and J. F. O'Brien, "Animating human athletics," in *Proc. of ACM SIGGRAPH*, (New York, NY, USA), pp. 71–78, 1995.

[10] L. Palmer and D. Orin, "Intelligent control of high-speed turning in a quadruped," *Journal of Intelligent & Robotic Systems*, vol. 58, pp. 47–68, 2010.

[11] D. Krasny and D. Orin, "Evolution of a 3D gallop in a quadrupedal model with biological characteristics," *Journal of Intelligent & Robotic Systems*, vol. 60, pp. 59–82, 2010.

[12] I. Mordatch, M. de Lasa, and A. Hertzmann, "Robust physics-based locomotion using low-dimensional planning," in *Proc. of ACM SIGGRAPH*, vol. 29, (New York, NY, USA), pp. 71:1–71:8, July 2010.

[13] R. Blickhan and R. Full, "Similarity in multilegged locomotion: Bouncing like a monopode," *Journal of Comparative Physiology A*, vol. 173, pp. 509–517, 1993.

[14] P. M. Wensing and D. E. Orin, "Generation of dynamic humanoid behaviors through task-space control with conic optimization," in *IEEE Int. Conf. on Rob. and Automation*, pp. 3088–3094, May 2013.